Eur. Phys. J. B **7**, 129–136 (1999)

THE EUROPEAN PHYSICAL JOURNAL B

EDP Sciences

Theoretical and computer simulation study of density fluctuations in liquid binary alloys

Ya. Chushak[a] and A. Baumketner

Institute for Condensed Matter Physics, 1 Svientsitskogo Street, Lviv 290011, Ukraine

Received: 27 February 1998 / Revised: 24 July 1998 / Accepted: 27 July 1998

Abstract. The dynamical properties of liquid alloys are investigated by means of memory function equations and molecular-dynamics simulation. A simple model for the second-order memory function in a binary liquid, based on Mori's memory function formalism, is proposed and applied in numerical calculations of the time correlation functions and dynamic structure factor of liquid $K_{0.7}Cs_{0.3}$ and $K_{0.3}Cs_{0.7}$ alloys. Obtained results are discussed in comparison with the results of computer simulations.

PACS. 61.20.Lc Time-dependent properties; relaxation – 61.25.Mv Liquid metals and alloys

1 Introduction

The microscopic dynamics of liquids can be described in terms of the density-density correlation function $F(k,t)$. Very extensive and detailed information is available on time-dependent correlations in monoatomic liquids through computer simulation and inelastic neutron scattering experiment [1]. A variety of theoretical approaches to this problem has also been developed, which may be broadly classified as based on either a generalized hydrodynamics description [2,3] or a memory function formalism [4,5]. In general, $F(k,t)$ is a complicated function of wavevector and time. On the other hand, the associated memory functions for $F(k,t)$ have simpler behaviours, so that a rather simple exponential approximation for the second-order memory function can reproduce fairly well the dynamic structure factor of monoatomic liquids in the (k,ω)-range that is accesible to the neutron-scattering experiment [6]. The analysis of molecular dynamics simulation [7–9] and neutron scattering data [10, 11] for monoatomic liquids had led to the conclusion that the relaxation time for the intermediate scattering function $F(k,t)$ is significantly longer than that for the memory function. Therefore, dynamical features can be analyzed more easy at the memory-function level rather than the correlation-function level.

Only recently has experimental and theoretical attention turned to more complex binary fluids. The most significant result has been obtained by Westerhuijs *et al.* [12] in a neutron scattering study of the dense He-Ne mixtures: the dynamic structure factors $S(k,\omega)$ are analyzed by fitting to a linear combination of Lorentzians and in terms of the extended hydrodynamic mode concept. It turns out that a minimum number of four Lorentzians centered at $\pm\,\omega_s^{(j)}(k),\ j=1,2$ is needed for an accurate fit. This analysis clearly shows the emergence of a high-frequency mode at intermediate and large wavevectors k. This higher-lying eigenmode at a frequency $\omega_s^{(1)}(k) > ck$ (where c is the velocity of sound of the mixture) is visible in $S(k,\omega)$. It can be associated with the fast motion of the lighter particles. The mode with $\omega_s^{(2)}(k) < ck$ is not directly visible in $S(k,\omega)$ and corresponds to slow motion of the heavier particles. A series of light-scattering experiments on dilute gas mixtures [13] together with a neutron scattering experiment on liquid Li_4Tl and Li_4Pb [14] have observed clear side peaks or shoulders in $S(k,\omega)$ at frequency $\omega_s(k) > ck$. The high-frequency collective mode at long wavelengths was also found by Bosse *et al.* [15] in a molecular-dynamics study of liquid $Li_{0.7}Pb_{0.3}$ alloy.

A theoretical analysis of dynamical processes in binary mixtures of hard spheres has been made by Campa and Cohen [16] in terms of the revised Enskog theory, which predicts that the fast sound vanishes at very long wavelength and that the slow sound merges with the hydrodynamic sound mode in this region. It was found that for low-density mixtures a fast mode exists if a mass ratio $m_2/m_1 \geq 5$, whereas for dense mixtures a larger mass ratio is necessary.

In a recent paper [17] the dynamical properties of liquid alloys have been investigated by means of the memory function equations. The viscoelastic approximation was extended for binary liquids. Within this model the dynamical properties of liquid $K_{0.7}Cs_{0.3}$ and $K_{0.3}Cs_{0.7}$ alloys are characterized by two diffusive and four propagating modes with dispersion $\pm\,\omega_s^{(j)}(k)$ and sound damping $\Gamma_s^{(j)}(k)$ ($j=$ 1,2). It is shown that the character of propagating modes depends strongly on the relative concentration of the light

[a] e-mail: ych@omega.icmp.lviv.ua

and heavy atoms in the alloy, in close analogy to the vibrational eigenmodes in substitutionally disordered crystalline and glassy mixtures.

In this contribution the density-density correlation functions and the associated second-order memory functions for these alloys are calculated in the viscoelastic approximation and compared with the computer simulation results. In the next section we briefly describe the general formalism of the memory function equations for time correlation functions of binary liquids and introduce some approximations which considerably simplify the structure of the second-order memory functions. Section 3 gives the details of the molecular dynamics simulation. The results of numerical calculations are presented in Section 4 and in Section 5 we discuss our results.

2 Theory

The quantities of interest here are the time-dependent correlation functions that are directly obtained from the molecular dynamic simulation

$$F_{ij}(\mathbf{k},t) = \langle \rho_i(\mathbf{k},t)\rho_j^*(\mathbf{k},0)\rangle. \tag{1}$$

The dynamical variable $\rho_i(\mathbf{k},t)$ ($i = 1, 2$) is the fluctuations of number density of the ith component at wavevector $\mathbf{k} \neq 0$ and is given by

$$\rho_i(\mathbf{k},t) = \frac{1}{\sqrt{N_i}} \sum_{p=1}^{N_i} \exp\left[i\mathbf{k}\mathbf{r}_p^{(i)}(t)\right] \tag{2}$$

where N_i is the number of particles of sort i and $\mathbf{r}_p^{(i)}$ is the position of particle p. Since the liquid is homogeneous, the time correlation functions are functions of the modulus $k = |\mathbf{k}|$ and time t. The elements of matrix $\mathbf{F}(k,0)$ are the partial static structure factors $F_{ij}(k,t=0) = S_{ij}(k)$.

The projection operators formalism of Mori [18] gives the equation of motion for $F_{ij}(k,t)$ in the form of the generalized Langevin equation (or memory function equation)

$$\frac{d}{dt}\mathbf{F}(k,t) = -\int_0^t d\tau \mathbf{M}^{(1)}(k,\tau)\mathbf{F}(k,t-\tau). \tag{3}$$

$\mathbf{M}^{(1)}(k,t)$ is the matrix of memory functions $M_{ij}^{(1)}(k,t)$. In Laplace space (characterized by argument z and denoted by a tilde) the solution of (3) can be written in the compact matrix form

$$\tilde{\mathbf{F}}(k,z) = [z\mathbf{I} + \tilde{\mathbf{M}}^{(1)}(k,z)]^{-1}\mathbf{F}(k,0), \tag{4}$$

where $\mathbf{I}$ is the unit matrix. Now the problem of calculation of the density-density correlation functions for arbitrary wavevector and time reduces to the evaluation of the corresponding memory functions. Furthermore, functions $M_{ij}^{(1)}(k,t)$ also satisfy an equation similar to (3).

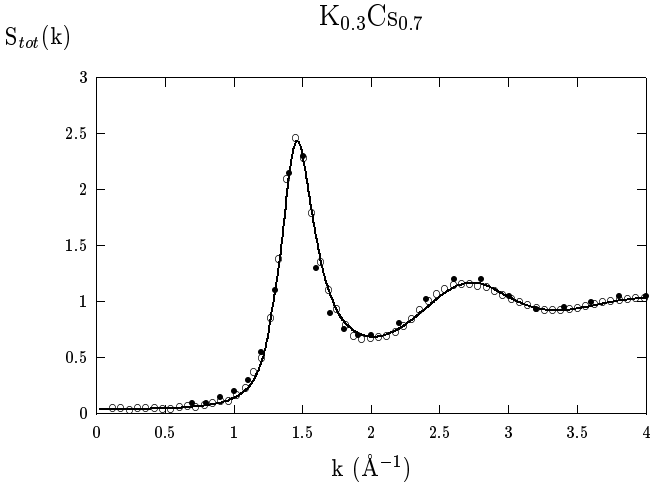

Fig. 1. Total (neutron weighted) static structure factors $S(k)$ for the $K_{0.3}Cs_{0.7}$ alloy. Solid lines: integral-equation results; open circles: MD data; full circles: experimental data [28].

A generalization of this leads to

$$\tilde{\mathbf{M}}^{(n)}(k,z) = [z\mathbf{I} + \tilde{\mathbf{M}}^{(n+1)}(k,z)]^{-1}\mathbf{M}^{(n)}(k,0). \tag{5}$$

One thereby obtains an infinite hierarchy of equations and the original aim of determining the density-density correlation functions can be achieved in closed form by truncating the hierarchy at a suitable point.

The initial values of memory functions $M_{ij}^{(n)}(k,t=0)$ are related to the frequency moments of the dynamic structure factors $S_{ij}(k,\omega)$

$$\langle\omega^{2n}(k)\rangle_{ij} = \int_{-\infty}^{\infty} \omega^{2n} S_{ij}(k,\omega)d\omega = (-1)^n \frac{d^{2n}}{dt^{2n}} F_{ij}(k,t)|_{t=0}. \tag{6}$$

The explicit expressions for $\langle\boldsymbol{\omega^0}\rangle$, $\langle\boldsymbol{\omega^2}\rangle$ and $\langle\boldsymbol{\omega^4}\rangle$ are given in [19]. These moments are expressed in terms of the equilibrium pair distribution functions and the interparticle potentials. The next frequency moments, *e.g.* $\langle\omega^6(k)\rangle_{ij}$ depend on the third and higher-order distribution functions. We shall, therefore, truncate the hierarchy (5) by introducing approximations on the second-order memory function, $\tilde{\mathbf{M}}^{(2)}(k,z)$ and this will allow us to fit the zeroth, second and fourth moments of the correlation spectra.

The expression for $M_{ij}^{(2)}(k,t)$ can be obtained by using the concepts of mode-coupling theory. In the latter framework the memory function is split into two contributions [20]: a short-time part is described as the effect of single uncorrelated binary collisions and a long-time tail is attributed to the non-linear couplings of the density and current fluctuations. The mode-coupling approach is able to account for the long-lasting features in binary liquids [21–23] whereas our understanding of the fast "binary" dynamics even in monoatomic systems at liquid density is not satisfactory [1].

Recently, a simplified method for the evaluation of the second-order memory functions was proposed. We briefly outline the method and for more details we refer the reader to [17]. In this approach, the third-order memory function, $\tilde{\mathbf{M}}^{(3)}(k,z)$ is appoximated by its value at $z=0$

$$\tilde{M}_{ij}^{(3)}(k,z) \approx \tilde{M}_{ij}^{(3)}(k,z=0) = \int_0^\infty M_{ij}^{(3)}(k,t)dt = M_{ij}^{(3)}(k). \tag{7}$$

Using the short-time behaviour of the first-order memory function $M_{ij}^{(1)}(k,t)$ the elements of the matrix $\mathbf{M}^{(3)}(k)$ were derived [17]

$$M_{ii}^{(3)}(k) = \frac{2}{\sqrt{\pi}}\sqrt{M_{ii}^{(2)}(k,0)}$$
$$M_{ij}^{(3)}(k) = \frac{2}{\sqrt{\pi}}\frac{M_{ij}^{(2)}(k,0)}{\sqrt{M_{jj}^{(2)}(k,0)}} \qquad (i \neq j). \tag{8}$$

The proposed approximations are in fact the analogue of the approximations proposed by Lovesey for monoatomic liquids [24]. In the case of monoatomic liquids the function $M^{(3)}(k)$ is directly connected with the relaxation time for the second-order memory function $M^{(3)}(k) = 1/\tau(k)$. For binary liquids the second-order memory functions $M_{ij}^{(2)}(k,t)$ are obtained as a linear combination of two exponentials

$$M_{ij}^{(2)}(k,t) = A_{ij}^1(k)e^{-t/\tau_1} + A_{ij}^2(k)e^{-t/\tau_2}, \tag{9}$$

where $1/\tau_1 = -z_1$, $1/\tau_2 = -z_2$ and z_1, z_2 are the roots of the equation

$$\det[z\mathbf{I} + \mathbf{M}^{(3)}(k)] = 0. \tag{10}$$

The amplitudes $A_{ij}^n(k)$ are related to the initial values $M_{ij}^{(2)}(k,0)$ and to $M_{ij}^{(3)}(k)$ (see [17]). Notice that all memory functions $M_{ij}^{(2)}(k,t)$ have the same relaxation times $\tau_1(k)$ and $\tau_2(k)$.

The foregoing assumptions provide then a simple, but approximate, description of the density fluctuations in binary liquids in terms of the static structure factors and of the fourth frequency moments of the correlation spectra. Such a description is invalid in the hydrodynamic region, where the energy density fluctuations should be included and where the two main relaxation times should be determined by the longitudinal viscosity and the thermal conductivity of the alloy.

3 Computer simulations

The systems we have studied are liquid $K_{0.7}Cs_{0.3}$ and $K_{0.3}Cs_{0.7}$ alloys at a temperature of $T = 373$ K and number densities $\rho = 0.01083$ Å^{-3} and $\rho = 0.0091$ Å^{-3}, respectively. The interatomic potentials have been calculated with a simple local empty-core model pseudopotential [25] using the dielectric screening function with the local-field corrections proposed by Ishimaru and Utsumi [26]. The simulation has been performed using a standard micro-canonical simulations technique with the usual periodic boundary conditions. The integration of the equations of motions was done by a 4th-order predictor-corrector Gear-algorithm with a time step $\Delta t = 2 \times 10^{-15}$ s. The runs have been performed over 50 000 time steps Δt for a system with $N = 2048$ particles. From the positions $\mathbf{r}_p^{(i)}(t), p = 1, ..., N_i$ of the ith sort particles along their trajectories, the Fourier transform of the density operator was determined for a given k-vector by means of (2). When we calculated $F_{ij}(k,t)$, the average is taken over all equivalent possible vectors $\mathbf{k}$ with $k = |\mathbf{k}|$.

Simultaneously, the static structure functions were obtained by means of integral-equation techniques based on a universal modelling of the bridge-functional [27]. The total (neutron weighted) static structure factor for $K_{0.3}Cs_{0.7}$ alloy is shown in Figure 1. Agreement between the calculated results (integral-equation (solid lines) and MD simulation (open circles)) and neutron scattering data [28] (solid circles) turns out to be very satisfactory.

4 Numerical results

Based on the interatomic potentials and the static structure factors the time correlation functions have been calculated within the framework of proposed approximation (8) and compared with the results of MD simulations.

The density fluctuations in binary liquids can be analysed in terms of Bhatia-Thornton-type number-number and concentration-concentration correlation functions [29] defined by

$$F_{NN}(k,t) = c_1F_{11}(k,t) + c_2F_{22}(k,t) + 2\sqrt{c_1c_2}F_{12}(k,t) \tag{11}$$

and

$$F_{CC}(k,t) = c_1c_2[c_2F_{11}(k,t) + c_1F_{22}(k,t) - 2\sqrt{c_1c_2}F_{12}(k,t)]. \tag{12}$$

The theoretical functions $F_{NN}(k,t)$ for both alloys in comparison with the results of MD simulation are plotted in Figure 2 and correlation functions $F_{CC}(k,t)$ are plotted in Figure 3. In both cases the theoretical curves follow closely the simulated ones. Some discrepancy between the theoretical and simulated $F_{ii}(k,t)$ for small-k is mainly due to our neglect of the temperature fluctuations. These fluctuations are important at $k \to 0$ and give an additional contribution to the long-time part of the time correlation functions [30].

At small-k $F_{NN}(k,t)$ has an oscillatory behaviour, similar to the density correlations in pure metals [7–9]. Such oscillations are associated with the propagation of sound-like excitations. As k increases $F_{NN}(k,t)$

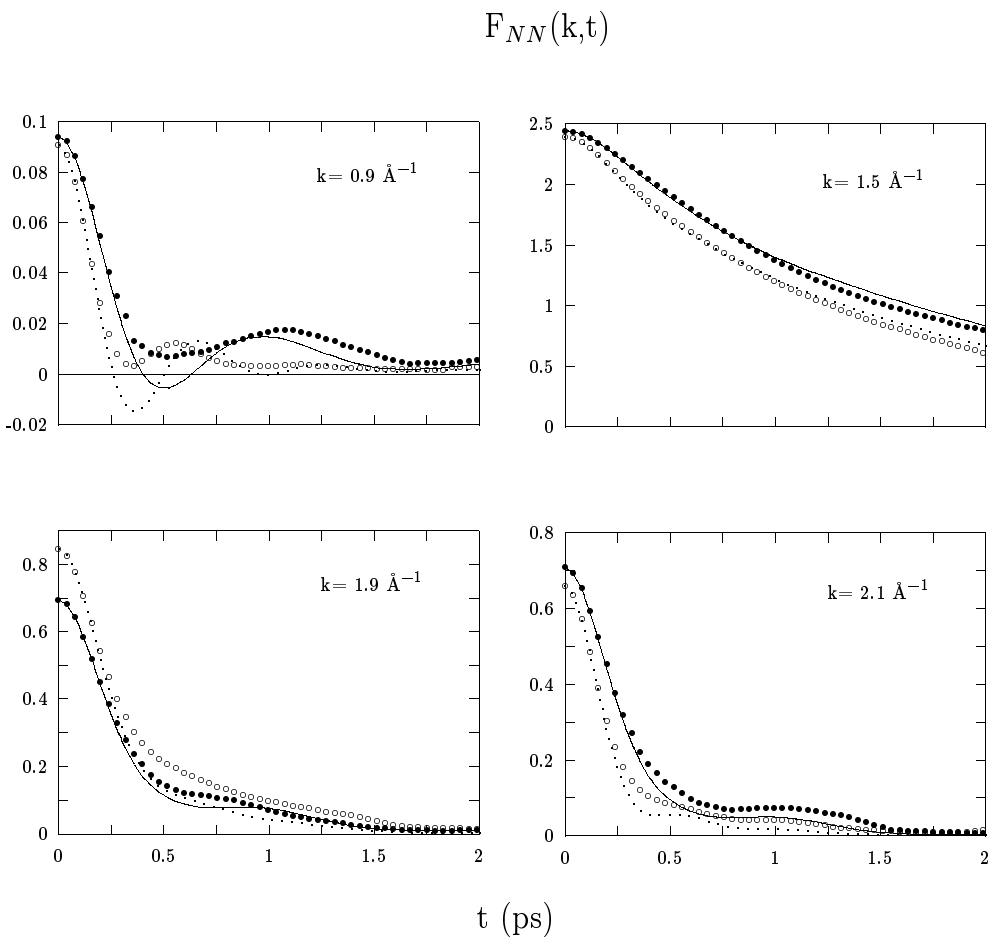

Fig. 2. Density-density correlation function $F_{NN}(k,t)$ for two alloys. Solid lines: theoretical results and solid circles: MD data for $K_{0.3}Cs_{0.7}$ alloy; dotted lines: theoretical results, and open circles: MD data for $K_{0.7}Cs_{0.3}$ alloy.

decays monotonically with time: the liquid alloy is not able to support any collective excitations. The half width of $F_{NN}(k,t)$ line shape has a maximum at the position of the main peak in $S(k)$ ($k \simeq 1.5$ Å^{-1}) and then decreases rapidly with wavevectors k. In contrast to $F_{NN}(k,t)$, there is no indication of any oscillations in the concentration-concentration correlation function $F_{CC}(k,t)$, that could be ascribed to concentration waves in liquid alloys. $F_{CC}(k,t)$ decreases monotonically with time at all wavevectors. Similar result was obtained by Jacucci and McDonald [31] in computer simulation of equiatomic Na–K alloy.

In the viscoelastic model for binary liquids the second-order memory functions are obtained as a linear combination of two exponentials (see Eq. (9)). Figure 4 shows the inverse of the relaxation times $1/\tau_i(k)$ for $M^{(2)}_{ij}(k,t)$ for both alloys. We also depicted the values of the reciprocal of the decay time $\tau(k)$ obtained in Lovesey's approximation [24] for pure K and Cs at the same temperature. This comparison shows that at intermediate and large wavevectors $\tau_i(k)$ for the two alloys considered in this study are very similar and follow closely the relaxation times of pure components. In the limit $k \to 0$ we see that $1/\tau_2(k)$ tends to zero like the pure components whereas $1/\tau_1(k)$ remains non-zero at $k = 0$ and have different values for different alloy compositions.

In Figure 5 we display the amplitudes of memory functions $A^n_{ij}(k)$ for two alloys under consideration. Solid circles and solid lines represent A^1_{ij} and A^2_{ij} for $K_{0.3}Cs_{0.7}$ alloy and open circles with dotted lines for $K_{0.7}Cs_{0.3}$ alloy, respectively. The second order memory function $M^{(2)}_{11}(k,t)$ is completely governed by $A^1(k)$ and $\tau_1(k)$ for both alloys and all wavevectors. The memory function $M^{(2)}_{22}(k,t)$ is determined by $A^2(k)$ only at intermediate and large wavevectors and is codetermined by two contributions at small-k. Furthermore, contribution from $A^1(k)$ becomes significant for K-rich composition. The non-diagonal elements of the second-order memory function matrix $M^{(2)}_{12}(k)$ and $M^{(2)}_{21}(k)$ are determined by two contributions for both alloys at all wavevectors.

The partial dynamic structure factors $S_{ij}(k,\omega)$ are the Fourier transforms of the corresponding time correlation functions $F_{ij}(k,t)$. To calculate $S_{ij}(k,\omega)$ we require the data of $F_{ij}(k,t)$ for long time intervals because the time correlation functions decay slowly – especially at small-k. Alternatively, we have fitted the simulated data to the model proposed in Section 2 and calculated

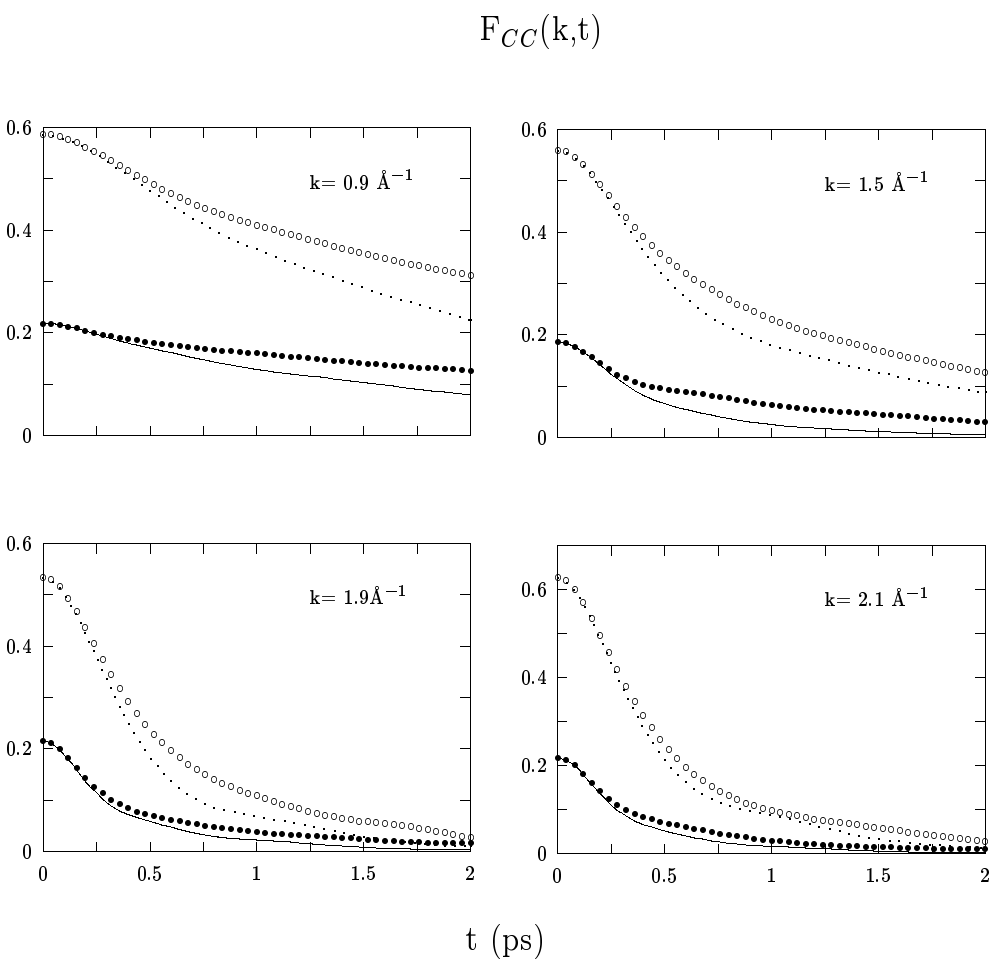

Fig. 3. Concentration-concentration correlation function $F_{CC}(k,t)$ at different wavevectors. Notations are the same as in Figure 2.

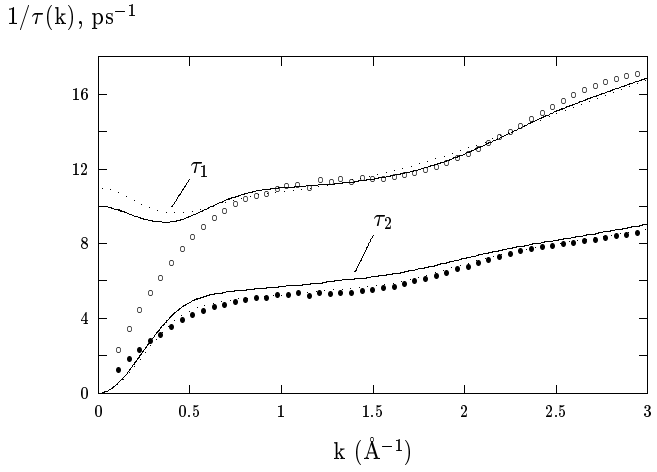

Fig. 4. Values of the reciprocal of the relaxation times $\tau(k)$. Solid lines: $K_{0.3}Cs_{0.7}$ alloy, dotted lines: $K_{0.7}Cs_{0.3}$ alloy; open circles: Lovesey's approximation for pure K; full circles: for pure Cs.

the Fourier transforms analytically. Figure 6 shows the total (neutron weighted) dynamic structure factor obtained from MD simulation in comparison with $S(k,\omega)$ calculated within the proposed model for $K_{0.7}Cs_{0.3}$ alloy. While the agreement between the theoretical and simulated curves is good, the shape of $S(k,\omega)$ at small-k is not too well described by the viscoelastic theory.

Based on equation (4) the dispersion relations $\omega_s(k) = iz(k)$ can be obtained as the solution of the equation

$$\det\left[z\mathbf{I} + \tilde{\mathbf{M}}^{(1)}(k,z)\right] = 0 \qquad (13)$$

which in our approach reduces to an equation of order six in z. These roots correspond to six modes: two of them turn out to be real, *i.e.* they describe purely diffusive (non-propagating) processes. The remaining four roots are two pairs of complex conjugate roots with the dispersion $\pm\ \omega_s^{(j)}(k)$ and the sound damping coefficients $\Gamma^{(j)}(k)$. The spectra of density fluctuations are represented as superpositions of six Lorentzians: two Lorentzians, associated with diffusive processes, form the central peak of the spectra. The other Lorentzians, centered around $\pm\ \omega_s^{(j)}(k)$ ($j = 1,2$), correspond to two propagating modes.

In Figure 7 we display the dispersion relations $\omega_s^{(j)}(k)$ calculated within the approximation (8) for both alloys in comparison with those calculated for the pure elements

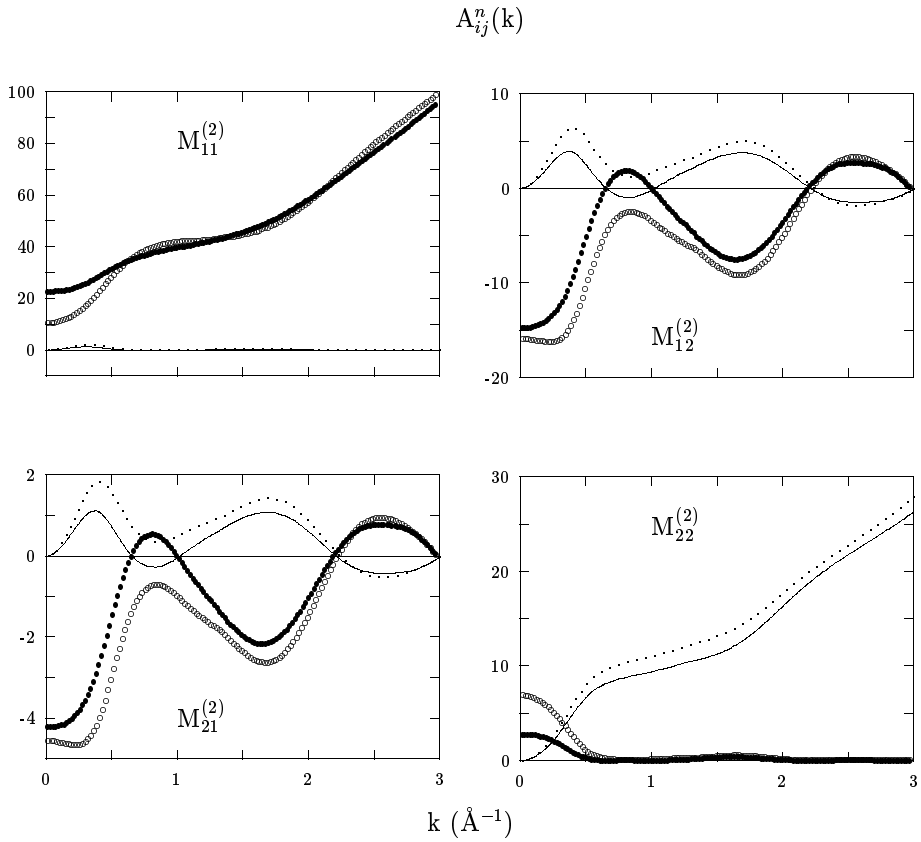

Fig. 5. Amplitudes of the second-order memory functions. Solid circles: A_{ij}^1, and solid lines: A_{ij}^2 for $K_{0.3}Cs_{0.7}$ alloy; open circles: A_{ij}^1, and dotted lines: A_{ij}^2 for $K_{0.7}Cs_{0.3}$ alloy.

K and Cs within the Lovesey's model. This comparison shows that propagating modes have a different behaviour in the two alloys. In the Cs-rich alloy the low-frequency mode follows closely the dispersion law of pure liquid Cs whereas at a majority concentration of K-atoms this mode follows the sound-wave dispersion of pure Cs only at small wavevectors and has a little dispersion at larger k. The high-energy mode has a finite frequency at $k \to 0$ for both alloys and follows the dispersion law of pure K at larger wavevectors only in K-rich alloy. The results presented in Figure 7 can be explained in terms of a simple impurity model [17]. In the zeroth order we have a "host" mode following the dispersion relations of pure component and a dispersion-less "impurity" mode. At the majority concentration of the lighter atoms the "impurity" mode occurs as a resonance within the frequency range of the host vibrations. At the point of intersection between the sound mode of the host atoms and the impurity mode, the interaction of the two modes leads to the formation of a hybridization gap. The strong interaction also leads to the strong damping of the high-energy mode in the long-wavelength limit. At a majority concentration of the heavier atoms an impurity mode lies above the spectrum of the host mode at all wavevectors and the interaction is much weaker.

5 Discussion

The analysis of neutron-scattering and molecular-dynamics simulation data for monoatomic liquids shows that the dynamic structure factor for different densities and k-values is well described as a sum of *three* Lorentzians [32]: the width of $S(k,\omega)$ is determined by extended heat mode, which is centered around $\omega = 0$, while the shape of $S(k,\omega)$ is codetermined by two extended sound modes. These sound modes are, for most values of k, found to be around values $\pm\ \omega \neq 0$. In the hydrodynamic limit ($k \to 0$) extended modes merge with the corresponding hydrodynamic modes.

In the case of binary liquids the linearized hydrodynamics describes the dynamic structure factor as a sum of *four* Lorentzians: the central peak is now a superposition of two Lorentzians, and a Brillouin doublet corresponds to propagating sound modes. It was shown [12,16] that such a set of dynamical variables is insufficient to describe $S(k,\omega)$ obtained from the neutron scattering for binary mixtures. An additional eigenmode associated with a nonconserved variable should be included into consideration. Therefore, the dynamic structure factor for binary liquids can be represented as a sum of *six* Lorentzians:

$$S_{ij}(k,\omega) = \frac{1}{\pi}\sum_{n=0}^{3} \mathrm{Re}\frac{A_{\pm}^n(k)}{i\omega + z_{\pm}^n(k)} \qquad (14)$$

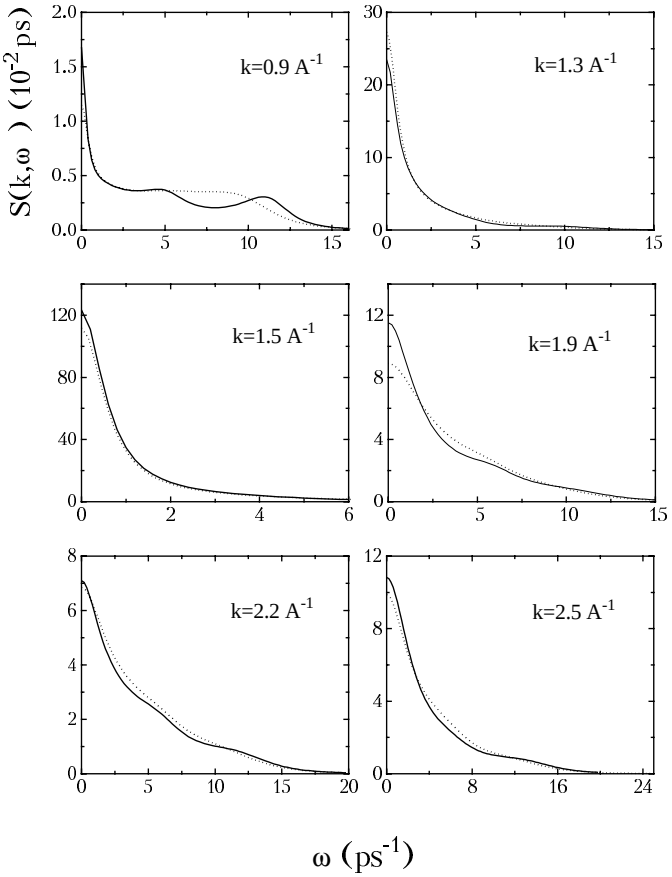

Fig. 6. Total (neutron weighted) dynamic structure factor $S(k,\omega)$ for $K_{0.7}Cs_{0.3}$ alloy. Solid lines: MD data; dotted curves: theoretical results.

where $A^0_\pm(k)$ and $z^0_\pm(k)$ are real and associated with two Lorentzians that describe the central peak of $S(k,\omega)$, whereas $A^n_\pm(k)$ and $z^n_\pm(k)$ ($n = 1, 2$) are the complex-conjugate pairs, *i.e.*, $A^n_- = A^{n\,*}_+$ and $z^n_- = z^{n\,*}_+$. They represent two propagating modes with the dispersion $\omega^{(n)}_s(k) = \mathrm{Im}\ z^n_\pm(k)$ and the corresponding damping $\Gamma^{(n)}_s(k) = \mathrm{Re}\ z^n_\pm(k)$.

Such a description of the dynamic structure factor involves twelve real parameters. On the other hand, the parameters $A^n_\pm(k)$ and $z^n_\pm(k)$ obey sum rules which follow from the short-time behaviour of $F_{ij}(k,t)$

$$\sum_{n=0}^{3} A^n_\pm(k)[z^n_\pm(k)]^m = \langle\omega^m(k)\rangle_{ij}. \qquad (15)$$

If we require that equation (15) be satisfied up to $m = 4$, the number of unknown parameters reduces to four. These parameters could be determined by least-squares fitting of the representation (14) to the MD data for $F_{ij}(k,t)$ or to the neutron-scattering data for $S(k,\omega)$. Alternatively, proposed in Section 2 approximation allows to calculate these parameters from the static structure factors and pair potentials. Obtained dispersion relations $\omega^{(n)}_s(k)$ are in good agreement with those derived from the fitting of MD data (Fig. 7). Comparison of the density-density correlation functions from theoretical calculations with those from MD-simulation shows, that the viscoelactic model is able to describe the density fluctuations in a range of wavelengths accessible to neutron scattering experiments. The theory is clearly worst at small-k, where the energy fluctuations should be included.

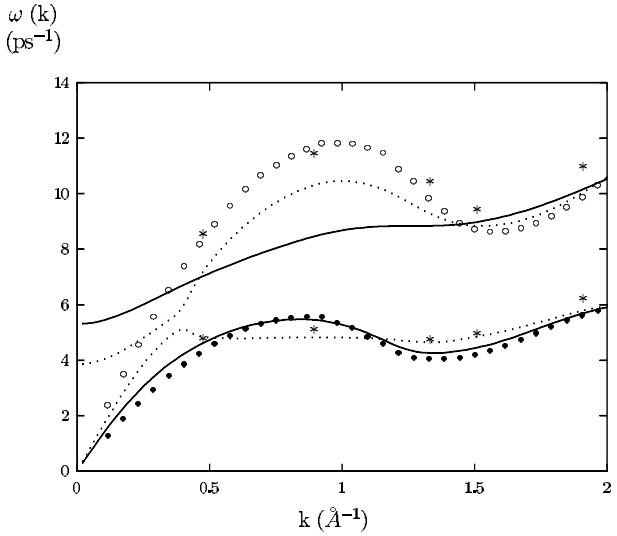

Fig. 7. Dispersion relations $\omega^{(j)}_s(k)$, $(j = 1, 2)$ for two alloys. Solid lines: $K_{0.3}Cs_{0.7}$ alloy; dotted lines: $K_{0.7}Cs_{0.3}$ alloy; ($*$): fitting of MD data for $K_{0.7}Cs_{0.3}$ alloy; ($\bullet$): pure Cs; ($\circ$): pure K.

This work has been supported by the National Ukrainian Academy of Sciences and by the Österreichische Bundesministerium für Wissenschaft und Forschung under Proj. No. GZ 45.385/2-IV/3A/94. Ya.Ch. would like to thank Dr. G.Kahl for very helpful discussions and the Institut für Theoretische Physik in Vienna for its hospitatity during the period when this work was performed.

References

1. U. Balucani, M. Zoppi, *Dynamics of the Liquid State* (Clarendon, Oxford, 1994).
2. R.D. Mountain, Adv. Mol. Relax. Process. **9**, 225 (1976); W.E. Alley, B.J. Alder, Phys. Rev. A **27**, 3158 (1983); I.M. de Schepper, P. Verkerk, A.A. van Well, L.A. de Graaf, Phys. Rev. Lett. **50**, 974 (1983).
3. T. Bryk, Ya. Chushak, J. Phys.-Cond. **9**, 3329 (1997).
4. J.P. Boon, S. Yip, *Molecular Hydrodynamics* (McGraw-Hill, New York, 1980).
5. J.-P. Hansen, I.R. McDonald, *Theory of Simple Liquids*, 2nd ed. (Academic Press, London, 1986).
6. J.R.D. Copley, S.W. Lovesey, Rep. Progr. Phys. **38**, 461 (1975).
7. F. Shimojo, K. Hoshino, W. Watabe, J. Phys. Soc. Jpn **63**, 141 (1994).
8. S. Kambayashi, G. Kahl, Phys. Rev. A **46**, 3255 (1992).
9. U. Balucani, A. Torcini, R. Vallauri, Phys. Rev. B **47**, 3011 (1993).
10. W. Gläser, P.A. Egelstaff, Phys. Rev. A **34**, 2121 (1986).

11. O. Söderström, U. Dahlborg, W. Gudowski, J. Phys. F: Met. Phys. **15**, L23 (1985).
12. P. Westerhuijs, W. Montfrooij, L.A. de Graaf, I.M. de Schepper, Phys. Rev. A **45**, 3749 (1992).
13. G.H. Wegdam, A. Bot, R.P.C. Schram, H.M. Schaink, H.M., Phys. Rev. Lett. **63**, 2697 (1989).
14. P.H.K. de Jong, P. Verkerk, C.F. de Vroege, L.A. de Graaf, W.S. Howells, S.M. Bennington, J. Phys.-Cond. **6**, L681 (1994).
15. J. Bosse, G. Jacucci, M. Ronchetti, W. Schirmacher, Phys. Rev. Lett. **57**, 3277 (1986).
16. A. Campa, E.G.D. Cohen, Phys. Rev. A **39**, 4909 (1989); *ibid.* A **41**, 5451 (1990).
17. Ya. Chushak, T. Bryk, A. Baumketner, G. Kahl, J. Hafner, Phys. Chem. Liq. **32**, 87 (1996).
18. H. Mori, H., Progr. Theor. Phys. **33**, 423 (1965).
19. D.L. Price, J.R.D. Copley, Phys. Rev. A **11**, 2124 (1975).
20. W. Götze, in *Liquids, Freezing and the Glass Transition* edited by D. Levesque, J.-P. Hansen, J. Jinn-Justin, (North-Holland, Amsterdam, 1991) p. 287; L. Sjögren, Phys. Rev. A **22**, 2866 (1980).
21. J.S. Thakur, J. Bosse, Phys. Rev. A **43**, 4378 (1991).
22. J.-L. Barrat, A. Latz, J. Phys.-Cond. **2**, 4289 (1990); M. Fuchs, A. Latz, Physica A **201**, 1 (1993).
23. J. Bosse, Y. Kaneko, Phys. Rev. Lett. **74** 4023 (1995); Y. Kaneko, J. Bosse, Molecular Simulation, **16** 249 (1996).
24. S.W. Lovesey, J. Phys. C **6**, 1856 (1973).
25. N.W. Ashcroft, Phys. Lett. **13**, 60 (1966).
26. S. Ichimaru, K. Utsumi, Phys. Rev. B **24**, 7385 (1981).
27. G.Kahl, B. Bildstein, Y. Rosenfeld, Phys. Rev. E **54**, 5391 (1996).
28. B.P. Alblas, W. van der Lugt, O. Mensies, C. van Dijk, Physica B **106**, 22 (1981).
29. A.B. Bhatia, D.E. Thornton, Phys. Rev. B **2**, 3004 (1970).
30. N.K. Ailawadi, A. Rahman, R. Zwanzig, Phys. Rev. A **4**, 1616 (1971).
31. G. Jacucci, I.R. McDonald, J. Phys. F: Metal Phys. **10**, L15 (1980).
32. A.A. van Well, P. Verkerk, L.A. de Graaf, J.B. Suck, J.R.D. Copley, Phys. Rev. A **31**, 3391 (1985); L.A. de Graaf, I.M. de Schepper, J. Phys.-Cond. **2**, 99 (1990).